The Colinear Helium Atom

Preben Bertelsen

An exam project for the course on classical and quantum chaos, finished 11/8 1995 supervised by Predrag Cvitanović and Gregor Tanner.

Abstract

The colinear model of the Helium is investegated. It is a sufficiently simple model which posseses a lot of the structure of real Helium. All cycles up to length 6 are determined by various methods, and the classical properties entering the zeta function is calculated numerically. Parts of the energy spectrum is determined by doing cycle expantion of the zeta function and determining its zeros by Newtons method. The results are compared with a cycle expansion including more cycles and full quantum solutions [4].

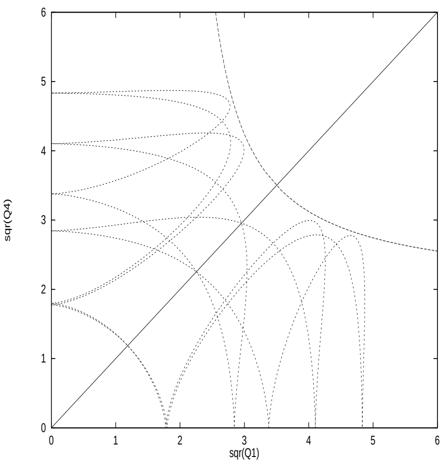

1 Equations of motion

In this section we reduce the classical 3-body problem with 9 degrees of freedom to a much simpler one with 2 degrees of freedom. This is done by three succesive coordinate transformations. Even though the model is simple, it is a very useful tool for describing real Helium. We use the model to calculate some parts of the helium energy spectrum (section 4).

1.1 The classical Helium atom

In general the three body problem is described by the Hamiltonian

$$\tilde{H} = \sum_{i=1}^{3} \frac{\tilde{\mathbf{p}}_i^2}{2m_i} + Z_1 Z_2 \frac{e^2}{\tilde{r}_{12}} + Z_1 Z_3 \frac{e^2}{\tilde{r}_{13}} + Z_2 Z_3 \frac{e^2}{\tilde{r}_{23}} = E \tag{1}$$

where Z_ie are the point charges, $\mathbf{p}_i$ the momenta, m_i the masses and r_{ij} the inter-particle distance. By scaling with the energy

$$\tilde{r}_{ij} = \frac{e^2}{\pm E}\hat{r}_{ij},\ \tilde{\mathbf{p}} = \sqrt{\pm E}\,\hat{\mathbf{p}}_i,\ \tilde{t} = \frac{e^2}{(\pm E)^{3/2}}\hat{t},\ \tilde{S} = \frac{e^2}{\sqrt{(\pm E)}}\hat{S} \tag{2}$$

we get a simpler Hamiltonian

$$\hat{H} = \sum_{i=1}^{3} \frac{\hat{\mathbf{p}}_i^2}{2m_i} + \frac{Z_1 Z_2}{\hat{r}_{12}} + \frac{Z_1 Z_3}{\hat{r}_{13}} + \frac{Z_2 Z_3}{\hat{r}_{23}} = \pm 1 \tag{3}$$

(where the $\pm$ is the sign of the energy E) and by introducing relative and centre of mass coordinates,

$$\mathbf{q}_1 = \hat{\mathbf{q}}_1 - \hat{\mathbf{q}}_3,\ \mathbf{q}_2 = \hat{\mathbf{q}}_2 - \hat{\mathbf{q}}_3,\ \mathbf{q}_3 = \hat{\mathbf{q}}_3 \tag{4}$$

$$\mathbf{p}_1 = \hat{\mathbf{p}}_1 - \hat{\mathbf{p}}_{CM},\ \mathbf{p}_2 = \hat{\mathbf{p}}_2 - \hat{\mathbf{p}}_{CM},\ \mathbf{p}_3 = \hat{\mathbf{p}}_{CM} = \hat{\mathbf{p}}_1 + \hat{\mathbf{p}}_2 + \hat{\mathbf{p}}_3 \tag{5}$$

we get the reduced Hamiltonian

$$H = \frac{\mathbf{p}_1^2}{2\mu_{13}} + \frac{\mathbf{p}_2^2}{2\mu_{23}} + \frac{\mathbf{p}_1\mathbf{p}_2}{m_3} + \frac{Z_1 Z_3}{r_1} + \frac{Z_2 Z_3}{r_2} + \frac{Z_1 Z_2}{r_{12}} = \pm 1 \tag{6}$$

where μ_{k3} are the reduced masses $\frac{m_k m_3}{m_k + m_3}$, r_i is the distance between electron nr. i and the core, r_{12} is the distance between the electrons. In order to smooth out the two-body collision singularities, $r_1 = 0, r_2 = 2$ and$r_{12} = 0$, we use the so called Kustaanheimo-Steifel transformation which conserves the Hamiltonian structure [2]. The motion is by assumption restricted to the invariant manifold $z_i = 0, p_{z_i} = 0$ (i.e. a trajectory starting in the plane stays there forever), so x_i and p_i are the (old) coordinates for electron nr. i:

$$x_1 = Q_1^2 - Q_2^2;\ y_1 = 2Q_1 Q_2;\ r1 = \sqrt{x_1^2 + y_1^2} = R_1^2 = Q_1^2 + Q_2^2$$

$$x_2 = Q_3^2 - Q_4^2;\ y_2 = 2Q_3 Q_4;\ r2 = \sqrt{x_2^2 + y_2^2} = R_2^2 = Q_3^2 + Q_4^2$$

$$p_{x_1} = \frac{Q_1 P_1 - Q_2 P_2}{2R_1^2};\ p_{y_1} = \frac{Q_2 P_1 + Q_1 P_2}{2R_1^2};$$

$$p_{x_2} = \frac{Q_3 P_3 - Q_4 P_4}{2R_2^2};\ p_{y_1} = \frac{Q_4 P_3 + Q_3 P_4}{2R_2^2};$$

$$d\tau = \frac{dt}{r_1 r_2}$$

where the new coordinates, momenta and time are $Q_i,\ P_i\ and\ \tau$. The new Hamiltonian is

$$\begin{aligned} H_r &= \frac{1}{8\mu_{13}} R_2^2(P_1^2+P_2^2) + \frac{1}{8\mu_{23}} R_1^2(P_3^2+P_4^2) \\ &+ \frac{1}{4m_3}[(Q_1Q_3+Q_2Q_4)(P_1P_3+P_2P_4) - (Q_1Q_4-Q_2Q_3)(P_1P_4-P_2P_3)] \\ &+ Z_1Z_3R_2^2 + Z_2Z_3R_1^2 + R_1^2R_2^2(1+\frac{Z_1Z_2}{R_{12}^2}) = 0 \end{aligned} \tag{7}$$

where $R_{12}^2 = r_{12}$ is given by

$$R_{12}^2 = \sqrt{(Q_1^2+Q_2^2)^2 + (Q_3^2+Q_4^2)^2 - 2(Q_1Q_3+Q_2Q_4)^2 + 2(Q_1Q_4-Q_2Q_3)^2} \tag{8}$$

1.2 The Colinear Helium model

A quick glance at equation (7) says, that it has to be simplified: The electron charges are: $Z_1 = Z_2 = -1$ and the charge of the core is $Z_3 = 2$. We assume, that the core is fixed, i.e. $m_3 = \infty,\ \mu_{13} = \mu_{23} = 1$. Furthermore, we assume that the 3 particles move along a common line with the electrons on opposite sides of the nucleus, the x-axis, which is an invariant manifold. This means that $Q_2 = Q_3 = P_2 = P_3 = 0$ and (7) reduces to:

$$\begin{aligned} H_{co} &= \frac{1}{8}(Q_4^2P_1^2 + Q_1^2P_4^2) - ZR_{12}^2 + Q_1^2Q_4^2(1+\frac{1}{R_{12}^2}) = 0 \\ R_{12}^2 &= Q_1^2 + Q_4^2 \end{aligned} \tag{9}$$

And the equations of motion are:

$$\begin{aligned} \dot{Q}_1 &= \frac{P_1Q_4^2}{4}\ \ \dot{P}_1 = 2Q_1[Z - \frac{P_4^2}{8} - Q_4^2(1+\frac{Q_4^2}{R_{12}^2})] \\ \dot{Q}_4 &= \frac{P_4Q_1^2}{4}\ \ \dot{P}_4 = 2Q_4[Z - \frac{P_1^2}{8} - Q_1^2(1+\frac{Q_1^2}{R_{12}^2})] \end{aligned} \tag{10}$$

We integrate these equations numerically using a fourth order Runge Kutta method in order to determine the phase space trajectories. Notice, that we also have to integrate $dt = d\tau(Q_1^2Q_4^2)$ to determine the period of a cycle (where τ is the old time variable). We have now reduced the number of degrees of freedom from 9 to 2, and the only singularity left, is the triple collision $r_{12} = 0$. There exist a one parameter family of orbits starting or ending on the triple collision, forming a stable and an unstable manifold [4]. This collision manifold generates a Markov partition of the Poincaré surface (see section 2.3). The symmetry with respect to the line $r_1 = r_2$, i.e. $Q_1^2 = Q_4^2$, corresponds to electron-electron interchange symmetry.

2 Cycle determination

To determine a cycle, one needs an iteration method which determines the phase space coordinates somwhere on the cycle. Section 2.1 describes how to find short cycles (up to sybol length 5), and section 2.2-2.4 gives a general method exploiting the Smale horseshoe dynamics in the Poincaré plane.

2.1 Short cycles

In order to find periodic orbits in phace space, or rather the configuration space (Q_1^2, Q_4^2), we must find some initial conditions (Q_1, Q_4, P_1, P_4), such that when we integrate the equations of motion (10), the trajectory returns to the starting point after some time. Because of the $e^- - e^-$ symmetry, our first attempt was to start on (and perpendicular to) the diagonal $Q_1 = Q_4$, where the equation $H_{co} = 0$ uniquely determines the magnitude of the momenta. Unfortunately, not all cycles cross perpendicular to the diagonal, but most short cycles can be found by starting perpendicular to either the diagonal, the Q_1-axis or the equipotential line determined by $H_{co} = 0$ and $P_1 = P_4 = 0$, depending on the symmetry of the cycle. For all three methods, the initial conditions have only one degree of freedom, so the cycle can be determined by a one-dimensional bisection method where you start integrating from e.g. the diagonal and check whether the trajectory returns to the diagonal above or below the starting point. We have implemented these three methods, and the short cycles in fig. 1 are determined this way. The cycles are drawn in the 'configuration space' (Q_1^2, Q_4^2) together with the diagonal $Q_1 = Q_4$ and the equipotential line $(H_{co} = 0,\ P_1 = P_4 = 0)$ corresponding to $(E = -1,\ \mathbf{p}_1 = \mathbf{p}_2 = \mathbf{0})$. In order to find longer cycles, we have to do some futher analysis of the phase space. This is done in the following sections.

2.2 Symbolic dynamics

In order to keep track of the different cycles, it is necessary to introduce symbolic dynamics. One way to do so is to label the intersections with the Q_1, Q_4 -axis by '0' and '1' respectively (the (0,1) symbolic dynamics). Although the (1,0) symbolic dynamics has its advantages (see section 2.3), It is convenient to introduce symbolic dynamics, which exploits the $Q_1 - Q_4$-symmetry. This can be done by letting '$+$' denote two consecutive intersections with the same axis, and '$-$' denote a change of axis. A string of symbols, e.g. $+--++-$, is called an itenerary. Due to this symmetry we can also define a *fundamental domain* below the diagonal by making a reflection each time the trajectory approaches the diagonal. All information, both classically and quantum mechanically, is conserved by this desymmetrisation.

2.3 The Poincaré Cut

Another way of visualizing the 4-dimensional colinear phase space

$$(Q_1, Q_4, P_1, P_4)$$

is to make a Poincaré-cut by plotting (Q_1^2, P_1) whenever $Q_4 = 0$. This is shown in fig. 2, where each area consists of initial conditions which have the same itenerary for the first three axis intersections. It turns out, although it so

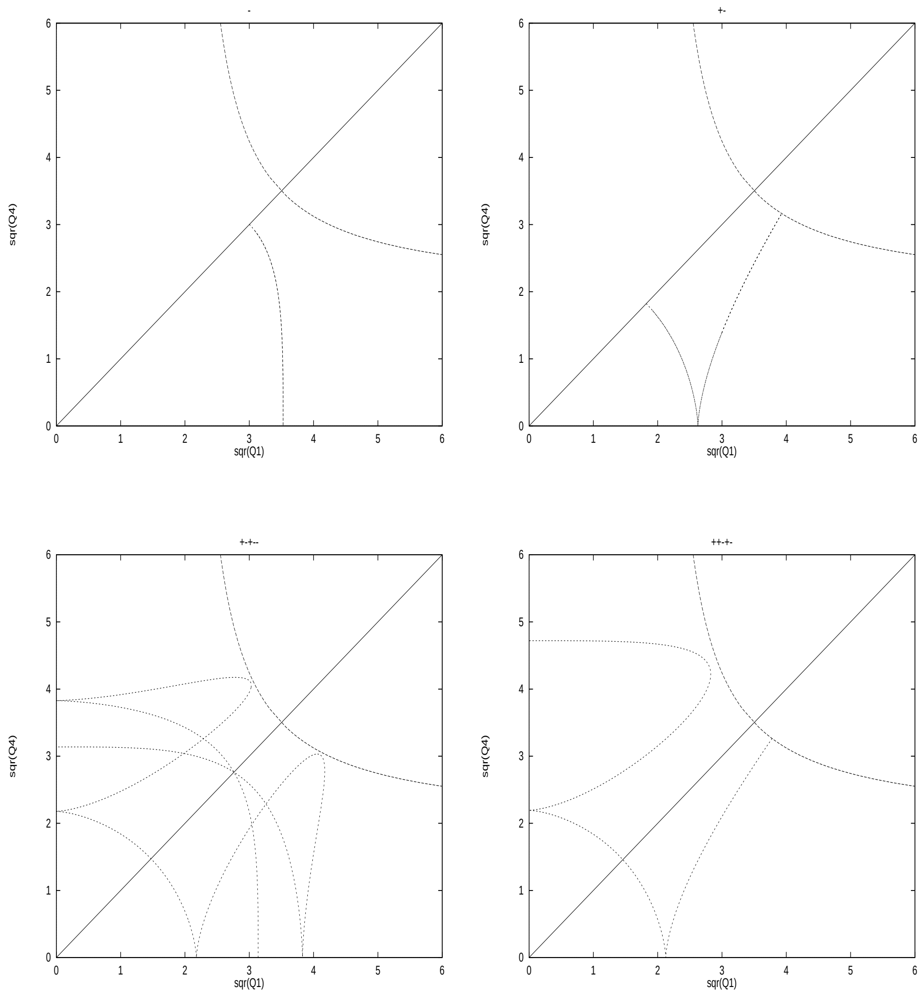

Figure 1: Four different cycles labelled with their $+,-$ itenerary. The diagonal $Q_1^2 = Q_2^2$ and the equipotential line (determined by $P_1 = P_2 = 0$ and $H_co = 0$) are drawn too. Three of the cycles are symmetric, '$++-+-$' is not. The two cycles to the right are drawn in the fundamental domain. All four cycles are retracing, i.e. they have a turning point where both momenta changes sign, so the trajectory moves 'back where it came from'. All four cycles can be determined by choosing initial conditions perpendicular to an axis. An example of a non-retracing cycle is given on the front page, the '$++-+--$' cycle, which can only be determined by the 2-dimensional search.

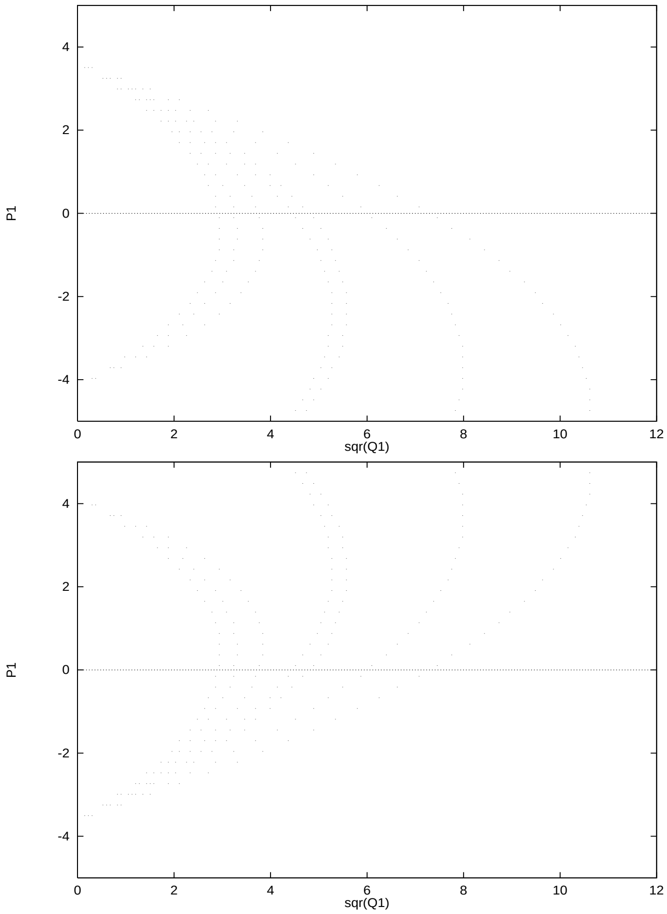

Figure 2: The Markov partitioning of the Poincaré plane. Each area contains those initial conditions which will hit some given axes during the next three intersections. The upper graph describes the future, while the lower part describes the past. The $(+,-)$-symbolic dynamics are similar to complete Smale horseshoe dynamics, while the (0,1) code is well ordered.

far has not been proven rigorously, that we are dealing with complete Smale horseshoe symbolic dynamics, i.e. there is a unique correspondence between periodic $(+,-)$-iteneraries and periodic orbits in the fundamental domain [1]. In the Poincaré cut we see eight strips, corresponding to the eight possible iteneraries of length 3. By labelling each area with it's (0,1)-itenerary, we see that the areas are well ordered. From left to right the order is '111', '110' ,'101', ..., '000', i.e. the binary number corresponding to the itenerary is decreasing with increasing Q_1^2.

By plotting areas corresponding to iteneraries of length 4, we observe that the areas in fig. 2 each split up in two areas, but the binary numbers corresponding to the areas are still decreasing. As the itenerary length grows further, the stripes becomes smaller and the number of stribes grows exponentially, converging to 'infinitely many stripes of width 0' as the itenerary length approches ∞. The lower part of fig. 2 is obtained by integrating 'backwards' in time, i.e. looking at the past instead of the future (for the same initial conditions). The only difference between the past and the future in the Poincaré plane is the sign of P_1 (the fact that both Q_4 and P_4 changes sign has no effect on the behavior of Q_4^2), so the lower part of fig. 2 is just a mirror image of the upper part.

A cycle has an infinite periodic itenerary, which can be divided into two infinite iteneraries, one describing the past and one describing the future of a certain initial condition. Each of the two iteneraries corresponds to a line in the Poincaré cut, and the cycle must therefore intersect the Poincaré cut at the intersection between these two lines, i.e. the cycle intersects the Poincaré cut in a single point. Actually a p-cycle intersects in p points because the infinite itenerary could have been divided in p different ways corresponding to p different initial conditions. Here it is important that the 'future-line' and the 'past-line' in the Poincaré plane are not parallel. This is not true everywhere in the Poincaré plane (e.g. for $P_1 < -3$ in upper part of fig. (2)), but it is true in the area where the cycles are located. The above observations shows that for small cycles, the intersection between the stable manifold (the past) and the unstable manifold (the future) yields the Smale horse shoe partition.

2.4 Two-parameter search

The fact, that we can define well ordered symbolic dynamics in the Poincaré cut, enables us to find cycles by an alternative method as described in [3]. The method is described below.

In general, well ordered symbolic dynamics can be defined for all complete Smale horseshoe maps. Given a binary iternerary $S = ...s_{-2}s_{-1}s_0 \cdot s_1 s_2...$, one can define the well ordered symbols (δ, γ), where γ is the symbolic past and δ is the symbolic future, as follows (for our purposes, we convert the $(+,-)$-itenerary to a binary itenerary by writing '0' instead of '+' and '1' instead of '$-$').

$$\omega_{i+1} = \begin{cases} w_i & \text{if } s_{i+1} = 0 \\ 1 - \omega_i & \text{if } s_{i+1} = 1 \end{cases} \qquad \omega_1 = s_1$$

$$\gamma(S) = 0.\omega_1\omega_2\omega_3... \tag{11}$$

$$\omega_{i-1} = \begin{cases} w_i & \text{if } s_{i-1} = 0 \\ 1 - \omega_i & \text{if } s_{i-1} = 1 \end{cases} \qquad \omega_0 = s_0$$

$$\delta(S) = 0.\omega_0\omega_{-1}\omega_{-2} \; ... \tag{12}$$

For a periodic itenerary, i.e. a cycle, we have $S = \overline{s_1 s_2 ... s_n}$ and

$$\gamma_c = \left(\sum_{i=1}^{2n} \frac{\omega_i}{2^i} \right) \frac{2^{2n}}{2^{2n} - 1} \qquad \delta_c = \left(\sum_{i=1}^{2n} \frac{\omega_{1-i}}{2^i} \right) \frac{2^{2n}}{2^{2n} - 1}$$

We begin each search by defining a rectangle in the Poincaré cut using the lower left corner $(Q^2_{1,min}, P_{1,min})$ and the upper right corner $(Q^2_{1,max}, P_{1,max})$. Then we calculate δ and γ for the middle point

$$(Q^2_{1,mid}, P_{1,mid}) = (\frac{Q^2_{1,min} + Q^2_{1,max}}{2}, \frac{P_{1,min} + P_{1,max}}{2})$$

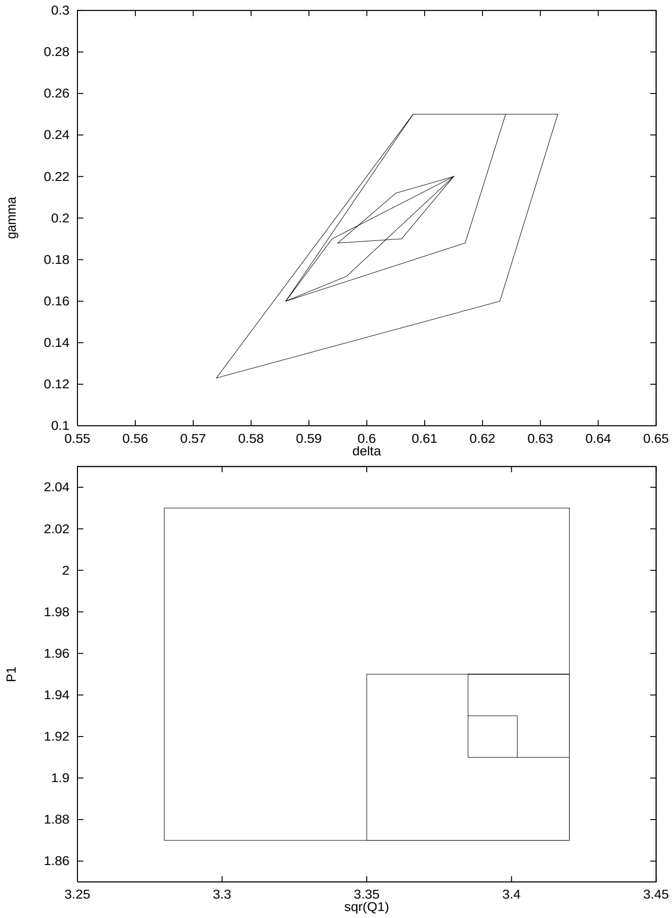

Figure 3: An illustration of the two parameter search method described in section 3.4. The large rectangle on the lower graph is the initial guess. By evaluating γ and δ in the middle point, one of the four quarters of the rectangle is chosen to be the next rectangle, etc. Notice that each correction in the (γ,δ)-plane corresponds to a correction in the opposite direction in the Poincaré plane. You can also see that the γ and δ axis are twisted compared to the Q_1^2 and $P1$ axis, and this is why the extra corrections are needed.

by integrating the initial condition $(Q^2_{1,mid}, 0, P_{1,mid}, P_2)$ (where P_2 is determined by $H_{co} = 0$) both forwards and backwards in time choosing s_i at every axis intersection and inserting in (11) and (12).

Now we need to know how γ and δ depends on the Poincaré cut variables Q_1^2 and P_1. In general one should define local γ and δ axis parallel to the stable and unstable manifolds, but fortunately γ and δ behaves nicely in large parts of the Poincaré plane, specially in the area in which the cycles are located. In fact, γ is decreasing in the P_1-direction and δ is decreasing in the Q_1^2-direction. Now we can choose a new smaller rectangle to be

$$\begin{array}{c} (Q^2_{1,mid}, P_{1,mid}), (Q^2_{1,max}, P_{1,max}) \ if \ \delta > \delta_c, \ \gamma > \gamma_c \\ (Q^2_{1,min}, P_{1,min}), (Q^2_{1,mid}, P_{1,mid}) \ if \ \delta < \delta_c, \ \gamma < \gamma_c \\ (Q^2_{1,mid}, P_{1,min}), (Q^2_{1,max}, P_{1,mid}) \ if \ \delta > \delta_c, \ \gamma < \gamma_c \end{array}$$

$$(Q^2_{1,min}, P_{1,mid}), (Q^2_{1,mid}, P_{1,max})\ if\ \delta < \delta_c,\ \gamma > \gamma_c$$

This iterative process is illustrated i figure 3. It might be nescessairy to do some corrections because the γ and δ axis don't follow the Q_1^2 and the P_1 axis, e.g. a change i P_1 causes a change in *both* γ and δ. Therefore, one corner of the rectangle is moved until the γ-value for the lower left corner is larger than γ_c and the δ-value for the this corner is larger then δ_c, and correspondingly for the upper right corner. This iteration scheme is continued until the size of the rectangle is sufficiently small. This method is very reliable, e.g. it converges to the right point (Q_1^2, P_1) even if you make a bad starting guess (the initial rectangle).

We have implemented this method and found several cycles, and their properties are in good agreement with [4]). Unfortunately, it does not converge as fast as the one dimensional search method mentioned in 2.1, so it might be nescessairy to combine this method with a 2-D Newton method for longer cycles. This is not implemented, because we only determined cycles up to code length 6.

3 Lyapunov exponents and winding numbers

Having found periodic orbits, we now wish to describe the linearized motion in the vicinity of their trajectories, i.e. calculate their Lyapunov exponents, etc. A local transformation recuces the problem to integrating two 2×2-matrices and finding their eigenvalues. This derivation follows the derivation in [1].

3.1 The Jacobian of the flow

In order to find Lyapunov exponents, we have to evaluate the Jacobian of the flow along the orbit. The equations of motion (10) have Hamiltonian structure, i.e. of the form:

$$\dot{q}_i = \frac{\partial H}{\partial p_i} \;\; \dot{p}_i = -\frac{\partial H}{\partial q_i} \quad i = 1, ..., n \tag{13}$$

This can be expressed in matrix representation if $x = (q, p)$ and $\mathbf{I}$ is the $(n \times n)$ unit matrix.

$$\dot{x} = \omega \frac{\partial H}{\partial x} \quad where\, \omega \;= \begin{pmatrix} 0 & \mathbf{I} \\ -\mathbf{I} & 0 \end{pmatrix}$$

The Jacobian describing the linearized motion along a phase space trajectory $x(t) = (q(t), p(t))$ is defined by $\delta x(t) = \mathbf{J}(t)\delta x(0)$ and the time evolution of $\mathbf{J}$ along the trajectory $x(t)$ is given by

$$\dot{\mathbf{J}}(t) = \mathbf{L}(t)\mathbf{J}(t) \quad where\;\; \mathbf{L}(t)_{ij} = \omega \left.\frac{\partial^2 H}{\partial x_i \partial x_j}\right|_{x(t)} \tag{14}$$

The Jacobian gives the time dependence of a displacement, but displacements in some directions have trivial time dependence. A displacement in the direction of the flow $\dot{x} = \omega \nabla H(x)$ evolves according to : $\delta x(t) = \frac{\partial x}{\partial t}(t)\delta t$ where δt is the initial displacement ($\delta x(0) = \frac{\partial x}{\partial t}(0)\delta t$). A displacement along the energy gradient ∇H has similar time evolution, because $\nabla H(x(t))\delta x(t) = \delta E$. Corresponingly, displacements in the directions of ∇L and $\omega \nabla L$ gives the trivial displacements $\delta x(t) = \delta x(0)$ and $\nabla L(x(t))\delta x(t) = \delta L$, respectively, where L is the angular momentum $L = \frac{1}{2}(Q_1 P_2 - P_1 Q_2 + Q_3 P_4 - P_3 Q_4)$.

3.2 Local transformation

The manifolds $E = -1$ and $L = 0$ are perpendicular with

$$\begin{aligned} \nabla H &= (H_{Q_1}, 0, 0, H_{Q_4}, H_{P_1}, 0, 0, H_{P_4}), \\ \nabla L &= (0, -P_1, P_4, 0, 0, Q_1, -Q_4, 0) \end{aligned} \tag{15}$$

where $H_{Q_1} = \frac{\partial H}{\partial Q_1}$ etc. This enables us to choose a local transformation $\mathbf{U}$ (i.e. an orthogonal basis), which seperates the trivial and the non-trivial parts of the Jacobian, reducing the 8×8 matrix to two 2×2-matrices.

$$\mathbf{U} = \left(\gamma_1^{\|}, \gamma_2^{\|}, \gamma_1^{\perp}, \gamma_2^{\perp}, \gamma_E, \gamma_t, \gamma_L, \gamma_\phi\right) = \tag{16}$$

$$\begin{pmatrix} \frac{-H_{P_4}}{R_H} & H_{Q_4} & 0 & 0 & \frac{H_{Q_1}}{R_H} & H_{P_1} & 0 & 0 \\ 0 & 0 & \frac{-Q_4}{R_L} & -P_4 & 0 & 0 & \frac{-P_1}{R_L} & Q_1 \\ 0 & 0 & \frac{-Q_1}{R_L} & -P_1 & 0 & 0 & \frac{P_4}{R_L} & -Q_4 \\ \frac{H_{P_1}}{R_H} & -H_{Q_1} & 0 & 0 & \frac{H_{Q_4}}{R_H} & H_{P_4} & 0 & 0 \\ \frac{-H_{Q_4}}{R_H} & -H_{P_4} & 0 & 0 & \frac{H_{P_1}}{R_H} & -H_{Q_1} & 0 & 0 \\ 0 & 0 & \frac{P_4}{R_L} & -Q_4 & 0 & 0 & \frac{Q_1}{R_L} & P_1 \\ 0 & 0 & \frac{P_1}{R_L} & -Q_1 & 0 & 0 & \frac{-Q_4}{R_L} & -P_4 \\ \frac{H_{Q_1}}{R_H} & H_{P_1} & 0 & 0 & \frac{H_{P_4}}{R_H} & -H_{Q_4} & 0 & 0 \end{pmatrix}$$

where $\gamma_t = \dot{x}$, $\gamma_E = \frac{\nabla H}{|\nabla H|^2}$, $\gamma_L = \frac{\nabla L}{|\nabla L|^2}$, $\gamma_\phi = \omega \nabla L$, $R_H = |\nabla H|^2$ and $R_L = |\nabla L|^2$. $\gamma_{1,2}^{\|}$ are two phase space vectors in the collinear plane perpendicular to each other and to γ_t and γ_E, and $\gamma_{1,2}^{\perp}$ are two phase space vectors perpendicular to the collinear plane.

The transformed Jacobian is $\tilde{\mathbf{J}}(x(t)) = \mathbf{U}^{-1}(x(t))\mathbf{J}(x(t))\mathbf{U}(x(0))$

$$\tilde{\mathbf{J}} = \begin{pmatrix} m_{11}^{\|} & m_{12}^{\|} & 0 & 0 & * & 0 & 0 & 0 \\ m_{21}^{\|} & m_{12}^{\|} & 0 & 0 & * & 0 & 0 & 0 \\ 0 & 0 & m_{11}^{\perp} & m_{12}^{\perp} & 0 & 0 & * & 0 \\ 0 & 0 & m_{21}^{\perp} & m_{22}^{\perp} & 0 & 0 & * & 0 \\ 0 & 0 & 0 & 0 & 1 & 0 & 0 & 0 \\ * & * & 0 & 0 & * & 1 & 0 & 0 \\ 0 & 0 & 0 & 0 & 0 & 0 & 1 & 0 \\ 0 & 0 & * & * & 0 & 0 & * & 1 \end{pmatrix}$$

where a star denotes a nonzero matrix element, which gives no contribution to the eigenvalues of $\tilde{\mathbf{J}}$. The time evolution of $\tilde{\mathbf{J}}$ is given by

$$\dot{\tilde{\mathbf{J}}} = \dot{\mathbf{U}}^{-1}\mathbf{J}\mathbf{U}_0 + \mathbf{U}^{-1}\mathbf{L}\mathbf{J}\mathbf{U}_0 = \tilde{\mathbf{L}}\tilde{\mathbf{J}} \ \textit{where} \ \tilde{\mathbf{L}} = \mathbf{U}^{-1}\dot{\mathbf{U}} + \mathbf{U}^{-1}\mathbf{L}\mathbf{U} \tag{17}$$

where $\mathbf{L}$ is given by (14), $\mathbf{U} = \mathbf{U}(x(t)), \mathbf{U}_0 = \mathbf{U}(x(0))$, etc.

$$\tilde{\mathbf{L}} = \begin{pmatrix} l^{\|}_{11} & l^{\|}_{12} & 0 & 0 & * & 0 & 0 & 0 \\ l^{\|}_{21} & l^{\|}_{12} & 0 & 0 & * & 0 & 0 & 0 \\ 0 & 0 & l^{\perp}_{11} & l^{\perp}_{12} & 0 & 0 & * & 0 \\ 0 & 0 & l^{\perp}_{21} & l^{\perp}_{22} & 0 & 0 & * & 0 \\ 0 & 0 & 0 & 0 & 1 & 0 & 0 & 0 \\ * & * & 0 & 0 & * & 1 & 0 & 0 \\ 0 & 0 & 0 & 0 & 0 & 0 & 1 & 0 \\ 0 & 0 & * & * & 0 & 0 & * & 1 \end{pmatrix}$$

3.3 Stability

The matrix elements for $\tilde{\mathbf{L}}$ are listed in the end of this section. The linearized motion in and perpendicular to the colinear plane is decsribed by the two independent (2×2)-matrices $\mathbf{m}^{\|}$ and $\mathbf{m}^{\perp}$. The motion in the colinear plane is unstable, so the eigenvalues of $\mathbf{m}^{\|}$ are real:

$$\Lambda = \frac{Tr(\mathbf{m}^{\|}) \pm \sqrt{Tr(\mathbf{m}^{\|})^2 - 4}}{2} \tag{18}$$

The Lyapunov exponent for a cycle, i.e. a periodic trajectory, is given by $\lambda_p = \frac{\log|\Lambda_p|}{T_p}$ where T_p is the cycle period and Λ_p is the largest eigenvalue of the Jacobian $\mathbf{m}^{\|}$ evaluated along the cycle trajectory. Λ_p is positive for hyperbolic orbits and negative for inverse hyperbolic orbits. The motion perpendicular to the plane is stable, which means that the eigenvalues of $\mathbf{m}^{\perp}$ are complex with absolute value 1: $\Lambda = e^{\pm i2\pi\nu}, 0 < \nu < 1$. The winding number for a cycle is the number of revolutions of the eigenvalue Λ in the complex plane along the cycle trajectory, i.e. $\nu + n$ where n is an integer.

The relevant matrix elements for $\tilde{\mathbf{L}}$ are:

$$\begin{aligned}
l^{\|}_{11} &= \frac{1}{R_H}(2H_{Q_1Q_4}(H_{Q_4}H_{P_1} + H_{Q_1}H_{P_4}) \\
&\quad +(H_{Q_1}H_{P_1} - H_{Q_4}H_{P_4})(H_{Q_1Q_1} - H_{Q_4Q_4} - H_{P_1P_1} + H_{P_4P_4})) \\
l^{\|}_{12} &= -2H_{Q_1Q_4}(H_{Q_1}H_{Q_4} - H_{P_1}H_{P_4}) \\
&\quad +(H^2_{Q_1} + H^2_{P_4})(H_{Q_4Q_4} + H_{P_1P_1}) + (H^2_{Q_4} + H^2_{P_1})(H_{Q_1Q_1} + H_{P_4P_4}) \\
l^{\|}_{21} &= \frac{1}{R^2_H}(2(H_{Q_1P_4} + H_{Q_4P_1})(H_{Q_4}H_{P_1} + H_{Q_1}H_{P_4}) \\
&\quad -(H^2_{P_1} + H^2_{P_4})(H_{Q_1Q_1} + H_{Q_4Q_4}) - (H^2_{Q_1} + H^2_{Q_4})(H_{P_1P_1} + H_{P_4P_4})) \\
l^{\|}_{22} &= -l^{\|}_{11} \\
l^{\perp}_{11} &= \frac{1}{R_L}(Q_1H_{P_1} + Q_4H_{P_4} - P_1H_{Q_1} - P_4H_{Q_4} + Q_1P_1(H_{Q_3Q_3} - H_{P_3P_3}) \\
&\quad +Q_4P_4(H_{Q_2Q_2} - H_{P_2P_2}) + (Q_1P_4 + Q_4P_1)H_{Q_2Q_3}) \\
l^{\perp}_{12} &= Q_1^2H_{P_3P_3} + Q_4^2H_{P_2P_2} + P_1^2H_{Q_3Q_3} + P_4^2H_{Q_2Q_2} + 2P_1P_4H_{Q_2Q_3} \\
&\quad +Q_1H_{Q_1} + Q_4H_{Q_4} + P_1H_{P_1} + P_4H_{P_4}
\end{aligned}$$

$$
\begin{aligned}
l_{21}^{\perp} &= \frac{1}{R_L^2}(Q_1^2 H_{Q_3Q_3} + Q_4^2 H_{Q_2Q_2} + P_1^2 H_{P_3P_3} + P_4^2 H_{P_2P_2} \\
&\quad +2Q_1Q_4 H_{Q_2Q_3} + Q_1 H_{Q_1} + Q_4 H_{Q_4} + P_1 H_{P_1} + P_4 H_{P_4}) \\
l_{22}^{\perp} &= -l_{11}^{\perp}
\end{aligned}
$$

We use these matrix elements to integrate the equations

$$
\dot{\mathbf{m}}^{\|} = \mathbf{l}^{\|}\mathbf{m}^{\|} \quad \dot{\mathbf{m}}^{\perp}\mathbf{l}^{\perp}\mathbf{m}^{\perp} \tag{19}
$$

along the cycle trajectory using a fourth order Runge Kutta method. The results obtained hereby, which are shown in the table below, are very similar to the results obtained by D. Wintgen et. al. [4]. Together with the action $S_p = T_p/\pi$, these are all the cycle properties we need to determine the zeta function. The first column contains the action T_p/π. The values differ from [4] by an amount of 0.00001. The reason for this could be, that our timestep dt is too high. The numerical work is done on a PC (486dx4 100MHz), which might not be fast enough. The second and the third row contains the stability exponent (i.e. the logarithm of the largest eigenvalue of the Jacobian) and the winding number, which both are identical with the results from [1] and [4].

4 Quantum Spectrum

Like Bohr quantized the helium atom using elliptic orbits, Guzwiller [5] etablished a connection between the quantum eigenvalues and the classical periodic orbits of a Hamiltonian system. The connection is made by Gutzwillers trace formula (or zeta funtion), which estimates the quantum energies using only classical properties of the periodic orbits. Following [1], we use the Gutzwiller - Voros zeta function and a cycle expansion to determine the near-colinear energy levels of Helium and compare them to full quantum solutions.

4.1 The zeta function

The Gutwiller-Voros zeta function has the general form [1] :

$$
Z_{qm} = \prod_p \exp\left[-\sum_{l=1}^{\infty} \frac{\exp\left[l(\frac{i}{\hbar}S_p(E) - i\alpha_p\frac{\pi}{2})\right]}{l\left|\det(\mathbf{1}-\mathbf{J}_p^l)\right|^{1/2}}\right]
$$

where $\mathbf{J}$ is the Jacobian and α_p is the Morse index along the trajectory, which equals two times the length of the itenerary of the cycle p. The dynamical zeta function is an approximate expression for the so called quantum classical determinant

$$
\det(E-\hat{H}) \propto \prod_n (E-E_n)
$$

which has zeros at the eigenstates of $\hat{H}$.

As described in section 3.2, the transformed Jacobian is decomposed into two 2×2 matrices concerning the motion in a perpendicular to the colinear

Code	Sp	$\log \Lambda_p$	ν	α
$-$	1.82900	0.6012	0.5393	2
$+-$	3.61825	1.8622	1.0918	4
$++-$	5.32615	3.4287	1.6402	6
$+--$	5.39451	1.8603	1.6117	6
$+++-$	6.96673	4.4378	2.1710	8
$++--$	7.04133	2.3417	2.1327	8
$+---$	7.25849	3.1124	2.1705	8
$++++-$	8.56618	5.1100	2.6919	10
$+++--$	8.64306	2.7207	2.6478	10
$++-+-$	8.93700	5.1563	2.7292	10
$++---$	8.94620	4.5932	2.7173	10
$+-+--$	9.02689	4.1765	2.7140	10
$+----$	9.07179	3.3424	2.6989	10
$+++++-$	10.13872	5.6047	3.2073	12
$++++--$	10.21673	3.0324	3.1594	12
$+++-+-$	10.57067	6.1393	3.2591	12
$+++---$	10.57628	5.6766	3.2495	12
$++-+--$	10.70699	5.3252	3.2520	12
$++--+-$	10.70699	5.3252	3.2520	12
$++----$	10.74303	4.3317	3.2332	12
$+-+---$	10.87855	5.0002	3.2626	12
$+-----$	10.91015	4.2408	3.2467	12

Table 1: Action, Lyapunov exponent for the motion in the colinear plane, winding number for the motion perpendicular to the plane and Morse index for all cycles up to code length 6.

plane. The denominator in the zeta function can thus be written as

$$\begin{aligned}|det(\mathbf{1}-\mathbf{J})|^{-1/2} &= (1-\Lambda_\perp)(1-\Lambda_\perp^{-1})(1-\Lambda_\parallel)(1-\Lambda_\parallel^{-1}) \\ &= \sum_{k,m=0}^{\infty} (\pm 1)^{lk} \left|\Lambda_\parallel\right|^{l(k+1/2)} |\Lambda_\perp|^{l(m+1/2)}\end{aligned}$$

where $\Lambda_\parallel = \pm e^{-\lambda}$ are real and $\Lambda_\perp = e^{-2\pi i\sigma}$ are complex with absolute value 1. The sum over l gives the expansion of a logarithm, so the zeta function is reduced to:

$$Z_{qm}(E) = \prod_{k=0}^{\infty}\prod_{m=0}^{\infty} \zeta_{km}^{-1} = \prod_{k=0}^{\infty}\prod_{m=0}^{\infty}\prod_{p}(1-t_p^{(k,m)})$$

where each periodic orbit has a weight given by

$$t_p^{(k,m)} = \exp\left[2\pi i\left(zS_p - 2(m+\frac{1}{2})\sigma_p\right) - (k+\frac{1}{2})(\lambda_p + \pi i\frac{\alpha_p}{2})\right] \qquad (20)$$

where $z = \frac{1}{\sqrt{-E}}$ (see eq. 2) is the effective quantum number. We are only interested in the leading zeroes of the zeta function, i.e. the zeroes which are closest to the real axis. Therefore it is enough to consider the case k=0. Furthermore, we only consider the states m=0 (i.e. no vibrations perpendicular to the collinear axis).

The cycle properties in table 1 is calculated in the fundamental domain, so different cycles have different contributions to the product. A symmetric cycle gives a contribution $(1-t_p^2)$ because its weigth in full space is two times its weigth in the fundamental domain. A non symmetric cycle gives a contribution $(1-t_p)^2$ since it has mirror image, which is a cycle with the same weigth. Therefore, the zeta function can be written as

$$\zeta_m^{-1} = \prod_{p,o}^{\infty}(1-t_p)^2 \prod_{p,s}^{\infty}(1-t_p^2)$$

or as a product of two zeta functions

$$\zeta_m^{-1} = \zeta_{m,+}^{-1}\zeta_{m,-}^{-1} \quad where$$

$$\zeta_{m,+}^{-1} = \prod_{p,o}^{\infty}(1-t_p)\prod_{p,s}^{\infty}(1-t_p) \quad \zeta_{m,-}^{-1} = \prod_{p,o}^{\infty}(1-t_p)\prod_{p,s}^{\infty}(1+t_p)$$

4.2 Cycle expansion

The best way to evaluate the infinite product $\zeta_{m,+}^{-1}$ is to expand it as a power series and regroupe the terms in a *curvature expansion* [4]. The terms are grouped in brackets where longer cycles are shadowed by products of shorter cycles. We have excluded the $'1'$ cycle, because it correspond to the situation where one electron is fixed with p=0 at r=∞ while the other electron bounces through the nucleus. Our cycle expansion will hereby reproduce states where both electrons stays close to the nucleus.

$$\begin{aligned}\zeta_{m,+}^{-1} &= 1 - t_0 - t_{01} - [t_{001} - t_0 t_{01} + t_{011}] \\ &\quad -[t_{0001} - t_0 t_{001} + t_{0011} - t_0 t_{011} + t_{0111}] + \ldots\end{aligned}$$

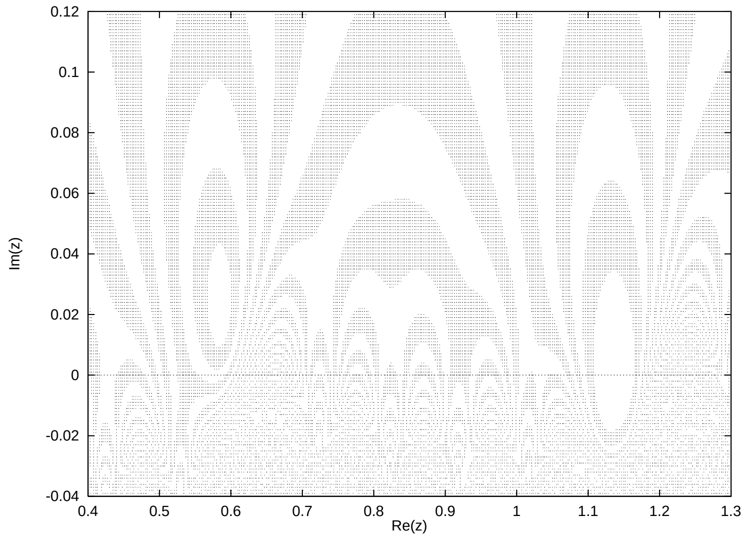

Figure 4: A contour plot, where each colored area corresponds to a certain range of the dynamical Zeta function. The large white areas surrounded by ellipses contain the z-values corresponding to the energy levels $(1,0)_1$ and $(2,1)_2$. Unfortunately, there are also many false zeros just below the real axis. For large negative imaginary part of z, the norm of the zeta function grows exponentially, so the bottom of the plot is a mess.

In our program we have made a curvature expansion up to cycle length 6. The zeroes of the zeta function is determined by a 2D Newton method (z is complex). We can choose the starting guess by looking at the contour plot (fig. 4) where you can see ellipses around the zeroes. But a faster method is to take e.g. 500 starting guesses along the real axis, check if they converge to a zero, and finally check whether the zero is sufficiently close to the real axis, e.g. if the imaginary part of z is in the interval [-0.02 , 0.02].

4.3 Energy spectrum

When both electrons are located in the near core region (as assumed earlier), the energy spectrum can be characterized as a set of different Rydberg series $E = -2/N^2$. The energy levels can be labeled by three quantum numbers $(N, K)_n$ where N is the principal quantum number for the inner electron, K (-(N-1) ¡= K ¡= (N-1)) counts for the different Rydberg series converging to the same energy threshold and n labels the states in the (N,K)-series [4]. K is related to the angle θ between the electron position vectors by

$$cos\theta \rightarrow \frac{-K}{N} \;\; forn \rightarrow \infty$$

The colinear configuration corresponds to $cos\theta = -1$, i.e. K=(N-1).

The results are seen in Table 2. Our calculations in the 'C6' column is compared to a cycle expansion including more cycles, to the 'cycle'-column, and to full quantum solutions (the 'QM'-column) [4]. The 'C6'-column consists of those zeros, whos imaginary part is in the interval [-0.020 ; 0.023]. Our spectrum is not perfect, as we have failed to find the $(4,3)_6$ level. Furthermore,

$(N,K)_n$	$C6$	$Cycle$	QM
$(1,0)_1$	2.919	2.932	2.904
$(2,1)_2$	0.787	0.778	0.778
$(2,1)_3$	0.586	0.585	0.590
$(3,2)_3$	0.353	0.353	0.354
$(3,2)_4$	0.282	0.282	0.281
$(4,3)_4$	0.198	0.199	0.201
$(4,3)_5$	0.166	0.166	0.166
$(4,3)_6$	$-$	0.151	0.151
$(5,4)_5$	0.130	0.129	0.129
$(5,4)_6$	0.109	0.109	0.110
$(5,4)_7$	0.100	0.101	0.100
$(6,5)_6$	0.0896	0.0895	0.0902
$(6,5)_7$	0.0777	0.0778	0.0780
$(6,5)_8$	0.0717	0.0717	0.0718
$(7,6)_7$	0.0655	0.0657	0.0663
$(7,6)_8$	0.0583	0.0583	0.0684
$(7,6)_9$	0.0540	0.0540	0.0541
$(8,7)_8$	0.0512	0.0510	0.0514
$(8,7)_9$	0.0453	0.0455	0.0455
$(8,7)_{10}$	0.0423	0.0423	0.0423

Table 2: The energy levels in atomic units obtained by our calculations (C6), a larger cycle expansion (cycle) and quantum solutions (QM). The cycle and QM columns are taken from [1]

we find 4 false zeroes which are as close to the real axis as the true zeros. They are located at E=0.759, E=0.208, E=0.00934 and E=0.0674. On the other hand, most of the energy levels are determined with an accuracy of 1%, so I think our cycle expansion will improve a lot by including more cycles in the curvature expansion (maybe the '+'-cycle).

5 Conclusion

The first part of the project, e.g. determining cycles is done succesfully, because a generel method is implemented, and only time trouble (both computer-time and real time!) prevented us from determining longer cycles. The next step was to calculate numerically the properties which enters the Gutzwiller zeta function. This was also done succesfully, and the results from [4] and [1] for the Lyapunov exponent and the winding number were reproduced. The determination of the energy spectrum is done and most of the singlet energies from [1] is reproduced. Our spectrum would probably be much better if more cycles are included in the cycle expansion, but unfortunately, we didn't have enough time to do this.

References

1. P.Cvitanović and G. Tanner, Lecture notes for course on classical and quantum chaos. NBI, Copenhagen 1995.
2. Klaus Richter, Semiklassik von Zwei-elektronen-atomen, Freiburg 1991.
3. Kai T. Hansen, Alternative method to find periodic orbits in chaotic systems. Freiburg.
4. D. Wintgen, A. Bürgers, K. Richter and G. Tanner, Semiclassic approach to Few-Body-Problems, Progress of th. ph. supp. no. 116, 1994, Freiburg.
5. M. C. Gutzwiller, Chaos in Classical and Quantum Mechanics, Springer, New York 1990